Acta Crystallographica Section A
Foundations of Crystallography
ISSN 0108-7673

Received 29 June 2009
Accepted 28 October 2009

A neutron interferometric measurement of a phase shift induced by Laue transmission

J. Springer,[a]* M. Zawisky,[a] H. Lemmel[a] and M. Suda[a,b]

[a]Vienna University of Technology, Atomic Institute, 1020 Vienna, Austria, and [b]Austrian Institute of Technology – AIT, Vienna, Austria. Correspondence e-mail: springer@ati.ac.at

The phenomenon of a neutron phase shift due to Laue transmission in a perfect crystal blade is discussed. Quantitative measurements of this phase shift are presented in the vicinity of the Bragg condition well in agreement with numerical calculations. The phase shift shows a strong angular sensitivity and might constitute an interesting opportunity for precision measurements of fundamental quantities like the neutron–electron scattering length or gravitational short-range interactions.

1. Introduction

Laue diffraction on a perfect crystal slab is the basis for perfect crystal neutron interferometry as it coherently splits the incoming neutron wave into a transmitted and a reflected component. Both wavefunctions can be calculated by dynamical diffraction theory. Here we want to focus on the phase of the transmitted beam, which shows a very peculiar behavior, different from an ordinary phase shifter described by the index of refraction (Lemmel, 2007). We refer to this phase as the 'Laue phase' rather than the 'dynamical phase' (Ioffe & Vrana, 2003; Wietfeldt *et al.*, 2006) as the latter might be misleading in the sense of distinguishing dynamical from topological phase shifts (Rauch & Werner, 2000). The Laue phase is effective on a much larger angular range than the Laue reflection itself. While the reflected amplitude is essentially zero if the beam angle differs more than a few arc seconds from the Bragg condition, the phase of the transmitted beam (Laue phase) still shows a remarkable difference from the index of refraction phase at angles some tenths of degrees off the Bragg condition. First related measurements on this feature have been presented in Graeff *et al.* (1978). The motivation for such measurements has additionally grown due to the fact that the Laue phase depends on the neutron–electron scattering length (Wietfeldt *et al.*, 2006; Ioffe & Vrana, 2003). As a first step we focus on measuring the Laue phase in principle and on developing suitable simulation programs. In a next step the accuracy should be improved to see if it is possible to extract fundamental quantities from a phase measurement.

2. Theory

Laue diffraction for neutrons is well understood within the theory of dynamical diffraction (Rauch & Werner, 2000; Werner, 1980). Recently, new approximations smoothly covering the transition range between the vicinity of the Bragg condition and the case of a simple phase shifter have been published (Lemmel, 2007); these are considered in the following. A neutron wave incident on a perfect crystal slab of thickness D with an angle θ close to the Bragg angle θ_B is split into a transmitted and a reflected beam (Fig. 1).

For our considerations the amplitude of the transmitted beam is of interest:

$$t(\eta) = \exp[-iA_0(1+\overline{\varepsilon}) - iA_H\eta]\Big\{\cos[A_H(1+\eta^2)^{1/2}(1+\varepsilon)] + \frac{i\eta}{(1+\eta^2)^{1/2}}\sin[A_H(1+\eta^2)^{1/2}(1+\varepsilon)]\Big\}, \quad (1)$$

where the abbreviations

$$A_{0,H} = \frac{Dkv_{0,H}}{2\cos\theta_B} = \frac{\pi D}{\Delta_{0,H}}$$
$$v_H = \frac{|V_H|}{E}, \qquad v_0 = \frac{V_0}{E}$$
$$V_0 = \frac{2\pi\hbar^2 N}{m}b_N, \qquad V_H = \frac{2\pi\hbar^2 N}{m}b_{atom}$$
$$\varepsilon = \frac{v_0}{2\cos^2\theta_B}, \qquad \overline{\varepsilon} = \varepsilon\frac{1+v_H^2/v_0^2}{2}$$
$$N = \text{atomic density}$$

are used. $\Delta_H = (2\pi\cos\theta_B)/(kv_H)$ denotes the *Pendellösung* length and η is a measure of the mis-set angle $\delta\theta = \theta_B - \theta$:

$$\eta = 2\sin\theta_B\big[\sin\theta_B - \sin(\theta_B - \delta\theta)\big]/v_H. \quad (2)$$

The coherent atomic scattering length (Sears, 1986)

$$b_{atom} = b_N - Z[1 - f(\mathbf{q})]b_{ne} \quad (3)$$

contains the nuclear (b_N) and the neutron–electron (b_{ne}) scattering length and the atomic form factor $f(\mathbf{q})$. At $\mathbf{q} \neq 0$ the Debye–Waller factor W (Butt *et al.*, 1988) leads to a further correction,

$$b_{atom} \rightarrow b_{atom}\exp(-W). \quad (4)$$

The amplitude factor [equation (1)] not only yields the intensity of the transmitted beam but also the phase shift the

neutron wave experiences in Laue transmission. The phase shift is given by the argument of the transmission factor,

$$\varphi_{\rm Laue}(\eta) \equiv \arg[t(\eta)], \tag{5}$$

and can be explicitly written as

$$\varphi_{\rm Laue}(\eta) = \varphi_{\rm Laue}(0) - A_H\eta + \arctan\left\{\frac{\eta}{(1+\eta^2)^{1/2}}\tan[A_H(1+\eta^2)^{1/2}(1+\varepsilon)]\right\}, \tag{6}$$

where $\varphi_{\rm Laue}(0) = -A_0(1+\bar{\varepsilon})$ plus a potential constant π from the use of the arctangent according to equation (5). The constant $\varphi_{\rm Laue}(0)$ is omitted in the following plots and the arctan function is continuously extended. A remarkable structure appears at the poles of the tangent term when $A_H(1+\eta^2)^{1/2}(1+\varepsilon) = (2n+1)\pi/2$ (Fig. 2). At these points the otherwise steadily increasing phase function shows small plateaus. These are related to the *Pendellösung* oscillations (Shull, 1968; Shull & Oberteuffer, 1972) and appear exactly at the minima of the transmitted intensity. In Fig. 3 the Laue phase over a large scale of $\delta\theta$ is shown.[1]

The Laue phase shows a strong dependence on η and therefore on $\delta\theta$. It is interesting to note that the angular dependence of the phase around the Bragg condition is to first order linear with respect to $\delta\theta$,[2]

$$\varphi_{\rm Laue}(\delta\theta) \simeq \varphi_{\rm Laue}(0) + \delta\theta(\pi D/d) + O(\delta\theta^3), \tag{7}$$

solely depending on the ratio between the crystal thickness and lattice-plane distance d. Hence the dependence on the atomic scattering length cancels at the Bragg condition as in the case far off, whereas it is the largest around the Darwin width of the reflection. Moreover, there is a high sensitivity at the positions of the *Pendellösung* plateaus (Fig. 2). The ratio D/d yields a remarkable angular sensitivity of the phase shift typically of the order 1° for $\delta\theta = 10^{-4}$ arcsec.

Equation (6) describes one single monochromatic plane wave with a certain mis-set angle $\delta\theta$. In a realistic experiment one has to deal with a certain angle and wavelength distribution, where the latter is of minor importance. This has to be taken into account for a proper calculation of the phase shift.

3. Measurements and numerical calculations

A first approach for a measurement of the Laue phase could consist of a rotation of a perfect crystal slab around the Bragg condition in an interferometer. Related experiments have been performed with neutrons (Graeff *et al.*, 1978) and X-rays (Hirano & Momose, 1996). There has also been a similar experiment for the case of a perfect crystal slab in Bragg geometry (Rauch, 1989). The experiments demonstrated qualitatively the increase of the phase shift as the Bragg condition is approached. However, close to the Bragg condition no data could be acquired due to a rapid destruction of the interference pattern, described by the visibility of the interferometer. The visibility is measured by scanning an auxiliary phase shifter in the interferometer and fitting the intensity of the O beam (Fig. 4). Usually we consider only the intensity integrated over the beam cross section. As is obvious from the cited experiments, maintaining the visibility close to the Bragg condition is one of the main challenges. There are mainly three effects influencing the visibility:

(1) A perfect crystal close to the Bragg condition leads to a fanning of the beam within the Borrmann triangle, with a

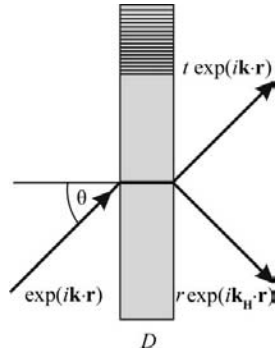

Figure 1
Sketch of a beam splitter in symmetrical Laue geometry. The transmission and reflection factors are denoted by r and t.

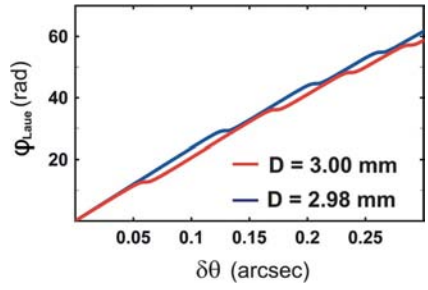

Figure 2
Laue phase for the silicon (220) reflection at $\theta_B = 45^\circ$ (λ = 2.72 Å) for two crystal thicknesses D. A fine structure depending on the ratio between crystal thickness and the *Pendellösung* length can be observed.

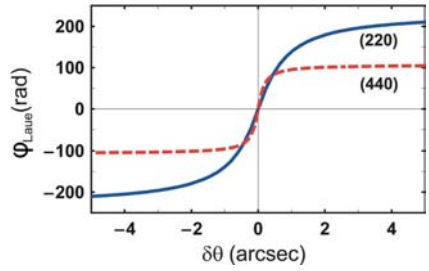

Figure 3
Plot of the Laue phase as a function of the deviation $\delta\theta$ from the Bragg angle ($\theta_B = 45^\circ$) for the silicon (220) (λ = 2.72 Å) and (440) (λ = 1.36 Å) reflections. The thickness of the Laue crystal is D = 3 mm.

[1] For large $\delta\theta$ the Laue phase asymptotically approaches the phase given by the index of refraction. In Fig. 3 it seems that each curve approaches different asymptotes for positive and negative $\delta\theta$. However, it can be shown that these asymptotes are separated exactly by a multiple of 2π, meaning that they are physically identical (Lemmel, 2007). One could also plot the phase modulo 2π or introduce one big jump *e.g.* at $\delta\theta = 0$. We prefer the given representation to emphasize the continuity of the phase function.

[2] This is only a good approximation as long as no *Pendellösung* structure is very close to $\delta\theta = 0$.

crucial influence on the focusing conditions in an interferometer.

(2) The strong angular dependence leads to a distinct phase distribution within the angular distribution (beam divergence) of the incoming beam, significantly reducing the visibility. This is similar to the influence of the wavelength distribution in the case of pure phase shifters. Here the coherence properties are strongly dominated by the pure geometrical angular dependence $\delta\theta$. Moreover, the phase shift averaged over the angular distribution is smaller than the phase shift for one single plane wave [equation (6)].

(3) Inserting and/or rotating crystal lamellas inside a neutron interferometer modifies the beam-path intensities. Asymmetric beam-path intensities reduce the visibility.

Hence one has to regard the whole system of beam, sample lamellas and interferometer in order to analyze defocusing effects and intensity changes in the two relevant beam paths. We have developed a simulation program (Lemmel, 2007) which allows one to compose arbitrary interferometer geometries. The incident beam is specified by the Bragg angle and the horizontal angular width (beam divergence) of the incoming beam. Lamellas can be rotated individually. Further crystal parameters like scattering lengths and type of Laue reflection can be chosen. The calculations are mono-energetic, but at the present stage this is not a severe limitation as calculations for slightly different wavelengths yield similar results. The divergent beam is calculated by a coherent superposition of stationary mono-energetic plane waves and a corresponding angle distribution,

$$\begin{aligned} g(\mathbf{k}) &= \delta(k - k_0) g_\theta(\delta\theta) \\ \psi(\mathbf{r}) &= (1/2\pi) \int \mathrm{d}^2k\, g(\mathbf{k}) \exp[i\mathbf{k}(\mathbf{r} - \mathbf{r}_0)] \\ &= (k_0/2\pi) \int \mathrm{d}\delta\theta\, g_\theta(\delta\theta) \exp[i\mathbf{k}_0(\mathbf{r} - \mathbf{r}_0)]. \end{aligned} \tag{8}$$

As an angular distribution a square function $g_\theta = \Theta(\delta\theta + \sigma_\theta) - \Theta(\delta\theta - \sigma_\theta)$, where $\Theta(x)$ is the Heaviside step function, with width $2\sigma_\theta$ and a Gaussian can be chosen, yielding similar results. The exact reflection curve of the perfect silicon crystal monochromator should be implemented for precision experiments. The transmitted and reflected wavefunctions after one single blade then read

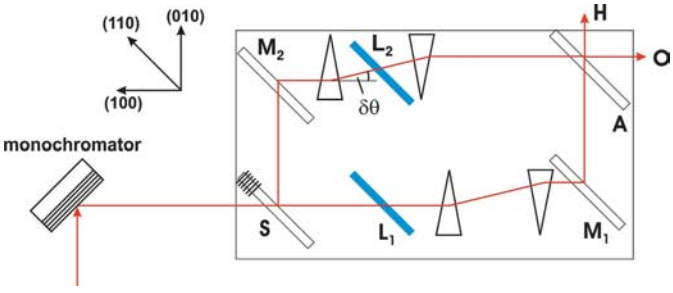

Figure 4
Perfect crystal monochromator and six-plate interferometer with beam deflection in front of lamella L_2 while L_1 [lamella thickness D = 2.959 (1) mm] remains at the exact Bragg condition. The beam path inside the lamellas and prisms is simplified.

$$\begin{aligned} \psi_t(\mathbf{r}) &= (k_0/2\pi) \int \mathrm{d}\delta\theta\, g_\theta(\delta\theta) t(\delta\theta) \exp[i\mathbf{k}_0(\mathbf{r} - \mathbf{r}_0)], \\ \psi_r(\mathbf{r}) &= (k_0/2\pi) \int \mathrm{d}\delta\theta\, g_\theta(\delta\theta) r(\delta\theta) \exp[i\mathbf{k}_\mathbf{H}(\mathbf{r} - \mathbf{r}_0)], \end{aligned} \tag{9}$$

where $\mathbf{k}_\mathbf{H}$ is the wavevector in the reflected direction and $r(\delta\theta)$ is the reflected amplitude analogous to equation (1). In the program the angular integration is substituted by the parameter η [equation (2)]. The exit beams (O, H) of the interferometer can be calculated by adding the contributions from the two beam paths after the last lamella and integrating over the beam cross section. Visibility and phase shifts are determined by applying auxiliary phase shifts between the two beam paths. Then the calculated intensities of the exit beams show sinusoidal oscillations and a sine fit yields the phase and visibility.

Applying this approach one finds that in the limit of large beam divergences the slope of the plane-wave result [equation (6)] is reduced by a factor of approximately three by phase averaging. On the other hand, for beam divergences σ_θ much smaller than the reflection width the calculated phase shift approaches the plane-wave result.

In our measurement a large six-plate interferometer (Zawisky *et al.*, 2002) has been used, where the middle lamellas act as perfect crystal samples. In this configuration, the focusing condition of the interferometer is guaranteed. Instead of rotating the lamellas (Wietfeldt *et al.*, 2006) the beam can be deflected in front of them using prisms (Ioffe & Vrana, 2003) as shown in Fig. 4. Here the phase shift obtained *via* beam deflection relative to L_2 is measured relative to lamella L_1 in the exact Bragg condition. The relevant deviation angle $\delta\theta$ in the scattering plane can be provided by rotation of the prisms around the incident beam direction by an angle α (Ioffe & Vrana, 2003). In this case the effective angular deviation is given by $\delta\theta = \delta \sin\alpha$, where δ is the total beam deflection by the prism.

The neutron interferometer has several remarkable features. It is actually the largest crystal interferometer (L = 23.5 cm) and its lattice planes are precisely oriented perpendicular to the lamella surfaces (asymmetry 13.5″ on average) (Zawisky *et al.*, 2009). This justifies the use of dynamical diffraction theory in symmetrical Laue geometry. In fact, for the chosen $\theta_\mathrm{B} = 45^\circ$ geometry not only the (220) but also two ($\bar{2}20$) reflections and the (040) reflection would be simultaneously excited (Hart, 1975; Hart & Lang, 1961). Nevertheless these reflections are in the dispersive arrangement with respect to the perfect crystal monochromator. The contribution in the present case is thereby negligible. In the case of precision measurements one should avoid these reflections by moving the setup sufficiently away from $\theta_\mathrm{B} = 45^\circ$.

The experiments were performed at the interferometer setup S18 at the ILL in Grenoble using the configuration shown in Fig. 4.

3.1. Visibility

Experiments at a Bragg angle of 45° were carried out for the (220) reflection (λ = 2.72 Å) and the (440) reflection (λ = 1.36 Å). Figs. 5 and 6 compare the measured visibility for these

two reflections with the calculated values. A rather good agreement between the predicted and measured visibility reduction was obtained. However, for both reflections a small shift of the visibility maximum relative to the expected zero position of the prisms was detected. We have analyzed several effects such as the non-ideal interferometer geometry (geometric errors up to 4 μm, but L1 and L2 have identical thickness within 1 μm accuracy) and the asymmetry of the lattice planes stated above, which however do not explain this effect. Recent analysis has shown that the Coriolis force from the Earth's rotation and the gravitational force acting along the beam trajectories explains most of this shift. As we found the same shift in our phase measurements the calculated visibility values have been adjusted accordingly.

3.2. Phase shift

Figs. 7 and 8 compare the measured phase shift with calculated values. The phase shifts show a linear behavior close to the Bragg condition but a nonlinear behavior further away. This is due to the *Pendellösung* structures in equation (6). The data for the (220) measurement show best agreement with the calculation if one assumes a beam divergence of $\sigma_\theta = 1.25''$. This corresponds approximately to the full reflection width of our perfect crystal monochromator. However, the (440) measurement shows a larger discrepancy between the best fit ($\sigma_\theta = 0.5''$) and the (440) reflection width of the monochromator ($\sigma_\theta \simeq 0.25''$). Here the fitted beam divergence is already in the region where a larger divergence would not significantly change the phase shift. The deviation is probably due to the difficult alignment between the lattice planes of the monochromator and the interferometer. A slight misalignment shows an equivalent effect to an enlarged beam divergence. This alignment and stability is more challenging for higher-order reflections, due to the reduced reflection width of the monochromator. Hence a better resolution of this alignment axis and/or the use of a mosaic crystal as monochromator with much larger beam divergence should lead to an improvement.

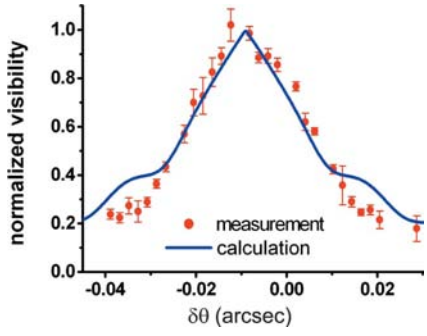

Figure 5
Measured visibility reduction for the (220) reflection compared with the calculated values, assuming an effective beam divergence of $\sigma_\theta = 1.25''$. The measured data are normalized to the maximum of a Gaussian fit. The calculated curve is shifted according to the measured offset.

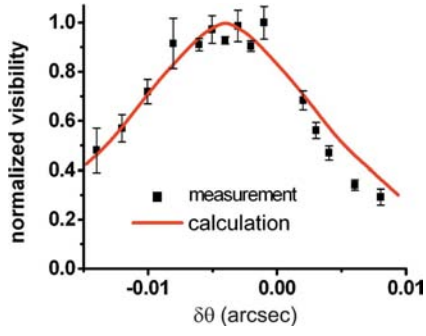

Figure 6
The measured visibility for the (440) reflection compared with the calculated visibility ($\sigma_\theta = 0.5''$). The measured data are normalized to the maximum of a Gaussian fit. The calculated curve is shifted according to the measured offset.

4. Discussion and outlook

Quantitative measurements of the phase shift due to Laue transmission have been performed in the vicinity of the Bragg condition and a comparison with accompanying numerical calculations has been presented. Good agreement concerning the detailed structure of the phase function could also be achieved. Moreover, despite the phase averaging a remarkable angular sensitivity of the phase shift remains. To obtain larger phase shifts, stronger deflecting prisms and/or thicker lamellas can be used. To overcome the visibility reduction at

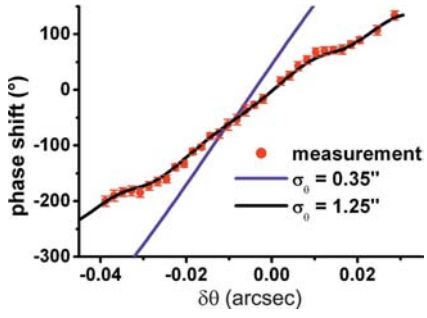

Figure 7
The measured phase shift for the (220) reflection compared with the best fitting beam divergence and another calculation ($\sigma = 0.35''$) that is already close to the phase shift of a single plane wave.

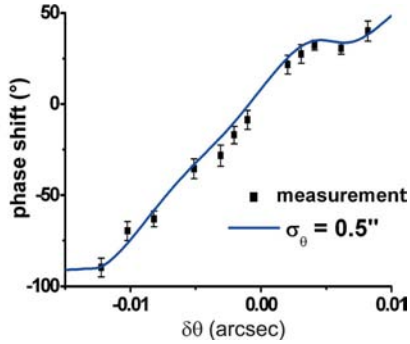

Figure 8
The measured phase shift for the (440) reflection compared with the best fitting beam divergence.

large beam deflections one can deflect the beams in front of both sample lamellas L_1 and L_2 but with slightly different deviations ($\delta\theta$ *versus* $\delta\theta + \delta$). The difference δ has to be small enough that high visibility is ensured. By this method in principle the slope of the Laue phase could be measured. Preliminary measurements have already shown that the visibility is maintained by this approach. A continuation of precise measurements related to the Laue phase is of general interest as it includes the neutron–electron scattering length and the Debye–Waller factor. Neutron interferometry could establish an independent method for the extraction of these fundamental neutron and crystal quantities. Finally, phase measurements around the Bragg condition have recently gained interest in the context of non-Newtonian gravity theories (Greene & Gudkov, 2007). In particular, the use of higher-order reflections as presented in this work is essential for these kinds of experiments. The high angular sensitivity of the phase shift could be used for the accurate measurement of beam deflections or crystal rotation. In this respect similar measurements could be interesting in the X-ray case. Furthermore, studying the related phase shifts also gives valuable information on the sensitivity of split-crystal neutron interferometers which have hitherto only been realized for X-rays (Bonse & te Kaat, 1968).

We thank R. Farthofer, A. Ioffe, U. Kuetgens, D. Petrascheck, H. Rauch and J. Summhammer for useful discussions. M. Hart contributed with helpful comments on the experiment. Financial support by the Austrian Science Foundation, project No. P18460-N16, is gratefully acknowledged.

References

Bonse, U. & te Kaat, E. (1968). *Z. Phys.* **214**, 16–21.
Butt, N. M., Bashir, J., Willis, B. T. M. & Heger, G. (1988). *Acta Cryst.* A**44**, 396–399.
Graeff, W., Bauspiess, W., Bonse, U. & Rauch, H. (1978). *Acta Cryst.* A**34**, s238.
Greene, G. L. & Gudkov, V. (2007). *Phys. Rev. C*, **75**, 015501.
Hart, M. (1975). *Proc. R. Soc. London Ser. A*, **346**, 1–22.
Hart, M. & Lang, A. R. (1961). *Phys. Rev. Lett.* **7**, 120–121.
Hirano, K. & Momose, A. (1996). *Phys. Rev. Lett.* **76**, 3735–3737.
Ioffe, A. & Vrana, M. (2003). *Appl. Phys. A*, **74**, 314–316.
Lemmel, H. (2007). *Phys. Rev. B*, **76**, 144305.
Rauch, H. (1989). *Nucl. Instrum. Methods Phys. Res. A*, **284**, 156–160.
Rauch, H. & Werner, S. A. (2000). *Neutron Interferometry*. Oxford: Clarendon Press.
Sears, V. F. (1986). *Phys. Rep.* **141**, 281–317.
Shull, C. G. (1968). *Phys. Rev. Lett.* **21**, 1585–1589.
Shull, C. G. & Oberteuffer, J. (1972). *Phys. Rev. Lett.* **29**, 871–874.
Werner, S. A. (1980). *Phys. Rev. B*, **21**, 1774–1789.
Wietfeldt, F. E., Huber, M., Black, T. C., Kaiser, H., Arif, M., Jacobson, D. L. & Werner, S. A. (2006). *Physica B*, **385–386**, 1374–1376.
Zawisky, M., Baron, M., Loidl, R. & Rauch, H. (2002). *Nucl. Instrum. Methods Phys. Res. A*, **481**, 406–413.
Zawisky, M., Springer, J., Farthofer, R. & Kuetgens, U. (2009). *Nucl. Instrum. Methods Phys. Res. A*, doi:10.1016/j.nima.2009.09.128.